Fusion Engineering and Design 221 (2025) 115389

Contents lists available at ScienceDirect

Fusion Engineering and Design

journal homepage: www.elsevier.com/locate/fusengdes

Thermo-mechanical analysis of a steering mirror with dielectric bulk for the ECRH system of DTT

Alfredo Pagliaro [a,*], Francesco Braghin [a], Alessandro Bruschi [b], Daniele Busi [a], Eliana De Marchi [c], Francesco Fanale [b], Gustavo Granucci [b,e], Afra Romano [d,e], Fabio Zanon [c]

[a] Politecnico di Milano, Department of Mechanical Engineering, Via Giuseppe La Masa 1, Milano 20156, Italy
[b] Institute for Plasma Science and Technology – National Research Council of Italy, Via Roberto Cozzi 53, Milano 20125, Italy
[c] Eni S.p.A., Piazzale Enrico Mattei 1, 00044 Roma, Italy
[d] ENEA, Technology for Nuclear Safety and Security Department, Via Enrico Fermi 45, Frascati 00044, Roma, Italy
[e] DTT S.C. a r.l, Via E. Fermi 45, Frascati 00044, Roma, Italy

ARTICLE INFO

Keywords:
Heat sink
Microwave technology
Steering mirror
Ceramic material
Dielectric material
CFD
FSI
ECRH

ABSTRACT

The steerable launcher mirrors, essential for directing microwave beams into the plasma, play a pivotal role in the Electron Cyclotron Resonance Heating (ECRH) system of the Divertor Tokamak Test (DTT) facility, currently under construction in Frascati, Italy. Due to the substantial heat loads acting on the mirrors, internal water-cooling channels are necessary to control temperature and deformation. A variable-depth complementary spiral cooling channel was considered in this study. A dielectric material with high thermal conductivity was selected as a potential candidate to reduce eddy currents, this mitigating magnetic torques and mechanical stress, while guaranteeing adequate cooling. Thermo-structural simulations (FSI) were conducted to assess the mirror's resistance to induced stresses, its deformations, and cooling performance. A transient analysis showed that thermal steady-state is the worst-case thermal loading condition during the entire experiment. Additionally, the thermo-structural behavior of various materials was analyzed to demonstrate the superior performance of the selected dielectric material. The cooling channel was subsequently adapted to a prototype mirror, on which CFD and FSI simulations were performed to validate the numerical model against future real-world experiments. Finally, crack propagation analysis confirmed the feasibility of using technical ceramics for the launching mirror, paving the way for dielectric materials in the ECRH system of DTT.

1. Introduction

The Divertor Tokamak Test (DTT) facility [1], currently being built in Frascati, Italy, is designed to investigate various divertor configurations under conditions relevant to DEMO. To ensure applicability to future fusion devices like DEMO, the divertors tested at DTT will be exposed to intense heat fluxes. Achieving this requires a powerful Heating and Current Drive system, integrating techniques such as Neutral Beam Injection, Ion Cyclotron Resonance Heating, and Electron Cyclotron Resonance Heating (ECRH). Specifically, the ECRH system will provide 32 MW of installed power, utilizing a 32 gyrotrons rated at 1 MW, operating at 170 GHz with a pulse duration of 100 s. A possibility to increase installed power is open, by considering the second batch of 16 gyrotron at 1.2 MW each [2]. The system includes 32 front-steering launchers, arranged across four machine sectors and featuring equatorial and upper antennas, with six and two launchers per sector, respectively [3]. The gyrotrons are organized into four clusters, each comprising eight sources. The power generated by each cluster is transmitted through a quasi-optical, evacuated multibeam transmission line [4] to two antennas positioned at the equatorial and upper ports of the DTT. The beams are directed into the plasma using independently adjustable mirrors [5]. During beam reflection, conductive materials experience ohmic losses, leading to significant thermal loads on the mirror surfaces. These thermal effects are further exacerbated by plasma radiation and nuclear loads. Due to the relatively long plasma pulse duration, an active water-cooling system is required to maintain mirrors temperature under control and minimize deformations [6]. Typically, cooling is achieved via dedicated internal channels. For instance, launcher mirrors in EAST [7] and KSTAR [8] incorporate S-shaped cooling channels, whereas W7-X [9,10] and some of the ITER [11]

* Corresponding author.
E-mail address: alfredo.pagliaro@polimi.it (A. Pagliaro).

https://doi.org/10.1016/j.fusengdes.2025.115389
Received 13 May 2025; Received in revised form 20 June 2025; Accepted 5 August 2025
Available online 13 August 2025

launcher mirrors adopt a spiral design. Other configurations employ serpentine cooling paths [12,13]. Each launcher consists of a fixed focusing mirror (M1) and a planar steering mirror (M2), both of which will be exposed to nuclear and radiative heat loads from the plasma, as well as additional heating from microwave absorption. The aim of this work is to analyse the thermo-mechanical stresses acting on the M2 mirror, investigating the feasibility of a Tungsten-coated dielectric substrate capable of eliminating the presence of eddy currents, thus preventing magnetic torques that exacerbate stress. Accordingly, electromagnetic analyses for dielectric components may be omitted, as the residual electrical conductivity is sufficiently low to prevent the occurrence of significant electromagnetic stresses on the component. In particular, this work focuses on the thermo-mechanical analysis of the dielectric substrate [14]. Among the possible alternatives for the substrate material, dielectric ceramics with high thermal conductivity – up to 170 W/(m·K) – like Silicon Carbide (SiC) and Aluminum Nitride (AlN) have been identified as potential candidates, considering both thermal and mechanical aspects. In particular, the case of SiC was analysed due to of its higher mechanical strength. Thermal performance of a new configuration of the M2 mirror based on a Variable-Depth Complementary Spiral (VDCS) cooling channel [15] has been simulated for various metallic materials and compared with the ceramic material. Transient thermo-structural analyses demonstrated that the steady-state condition is the most critical scenario along the entire experiment, enabling to focus the computationally expensive Fluid-Structure Interaction (FSI) simulations on the steady-state case.

Subsequently, different materials are compared in terms of thermo-mechanical resistance to the foreseen thermal loads, and a crack propagation analysis was conducted, based on the fracture toughness of the ceramic material. Finally, the customized VDCS cooling channel was adapted to a prototype mirror geometry with a distinct shape and size, to be tested experimentally for assessment and validation purposes. Computational Fluid-Dynamic (CFD) and FSI simulations were performed on the test mirror configuration to assess thermo-mechanical performance.

2. M2 mirror

The steerable mirrors (M2) of all DTT launchers will have the same geometry to increase modularity. The M2 mirror is an elliptic plate with a minor axis of 69 mm, a major axis of 132 mm and a thickness of 10 mm, as illustrated in Fig. 1 [4]. The thickness is selected to ensure adequate structural strength; in this study, a minimum thickness of 2 mm was considered for both the frontal and rear plates, while 6 mm are occupied in-between by internal channels. The internal VDCS channel geometry, characterized by a single inlet and a single outlet with a diameter of 5.5 mm, was designed to maximize heat exchange [15] by increasing the surface area, allowing the use of materials with lower thermal conductivity with respect to copper, such as advanced ceramic like SiC or AlN. The cooling channel features a Gaussian shape combined with a sinusoidal function to accelerate the fluid in the central section, enhancing heat exchange between the solid and water. The fluid is decelerated in the peripheral region to mitigate pressure losses along the conduit. This approach resulted in satisfactory thermal performance, enabling the use of the selected ceramic materials [15]. Additionally, the mirror, including the internal channel, would be made entirely of dielectric material, and the possibility of manufacturing the mirror using 3D printing technologies with the selected ceramics is currently under evaluation. The opportunity offered by dielectric materials, specifically ceramics, is that of suppressing the electromagnetic loads on the mirror and on the supporting system both during operation and, most importantly, during disruptions. The tokamak's magnetic fields are constantly changing, from plasma formation and ramp-up to when the plasma current is ramped down. The dynamic behaviour of the magnetic fields induces eddy currents in nearby conductors such as metallic structures or components. Any un-mitigated instability in the plasma, like

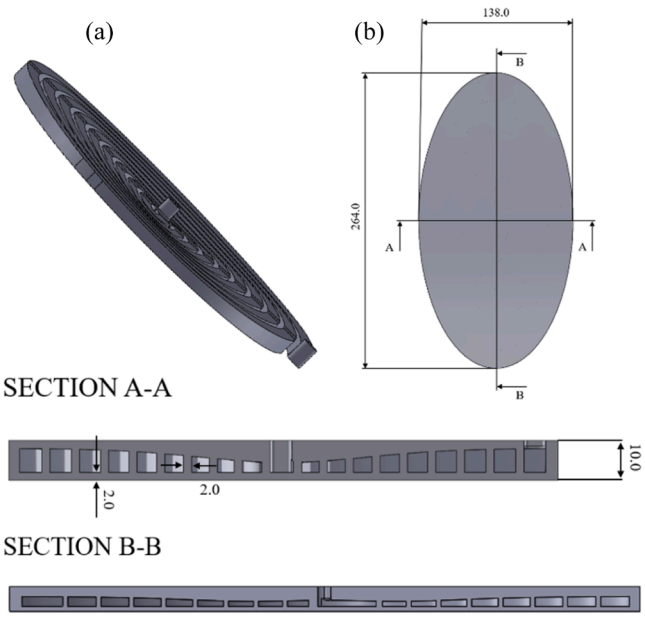

Fig. 1. (a) Internal variable-depth complementary spiral (VDCS) cooling channel. (b) M2 Mirror size and section view.

magnetohydrodynamic (MHD) instabilities, can cause abrupt changes in the magnetic field configuration called *disruptions*. These variations create strong transient magnetic field fluctuations, inducing high currents in surrounding metal parts [14]. The main possible consequence is the interaction between the magnetic fields and eddy currents generates Lorentz forces, creating mechanical stress on the tokamak's metallic structures. These forces can be substantial, especially during disruptions, potentially leading to structural failure or fatigue over time. As mentioned in Section 1, Tungsten-coated SiC was identified as a potential candidate as M2 mirror material. Specifically, a conservative value of thermal conductivity equal to 100 W/(m·K) was considered. Additionally, the M2 mirror was modeled including two lateral pins to simulate the constraints imposed by the supporting system and allowing for a more accurate estimation of the thermo-mechanical stresses. Fig. 2 shows the configuration of the M2 mirror including the supports and the customized cooling channel.

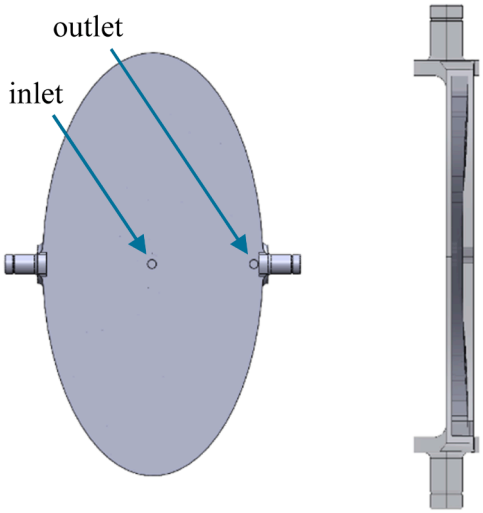

Fig. 2. M2 mirror with lateral supports.

3. Steady-state thermo-mechanical analysis of M2

Thermal simulations are conducted using STAR-CCM+ with the Finite Volumes Method (FVM) [16]. As shown in Fig. 3a polyhedral mesh is specifically created for the geometry under examination, tuning the turbulence model parameters to maximize the accuracy of the results [15,17]. The crucial parameters to study are the intensity and the turbulence length scale, as well as the boundary layer required to accurately capture the fluid dynamic behaviour at the wall.

The following boundary conditions are set for the problem:

- the inlet flow rate is set at 10 l/min;
- the inlet temperature is set at 50 °C;
- the outlet pressure is set at 4 bar;

The heat fluxes from microwaves P_{mw}, plasma irradiation P_{pl} and volumetric neutron heating P_n are included as follows:

- $P_{mw} = \frac{2Q}{\pi w_x w_y} e^{-2\left(\left(\frac{x}{w_x}\right)^2 + \left(\frac{y}{w_y}\right)^2\right)}$ MW/m^2
- $P_{pl} = 0.1768$ MW/m^2
- $P_n = 10$ kW/m^3

With beam power $Q = 1$ MW, and beam radii w_x and w_y evaluated for a 58° incident angle (worst case scenario) equal to 43 mm and 81.1 mm, respectively, resulting in a central peak power density of 1.874 MW /m^2 [15,18,19]. Furthermore, it is assumed that the presence of the micrometric Tungsten coating has no effect on the thermal performance of the mirror, given its very low thermal resistance. In Fig. 4, the thermal and fluid dynamic results at steady state are shown [15]. Both the maximum mirror temperature of 138 °C and the maximum pressure of 8.89 bar are acceptable, given a maximum pressure limit of 12 bar.

The structural analysis of M2 is carried out through a Fluid-Structure-Interaction (FSI) simulation, where the fluid dynamic part is coupled with the thermo-structural aspect of the component to obtain a comprehensive set of output fields. The simulations are conducted using ANSYS with the Mechanical APDL tool, solving the problem through Finite Elements Method (FEM). The same geometry used in STAR-CCM+ is imported into ANSYS; a tetrahedral mesh is created, as shown in Fig. 5 (a), consisting of triangular faces. The pressure field from the fluid acting on the internal wall of the cooling channel and the temperature field of the solid component are imported.

The following mechanical boundary conditions are imposed on the lateral supports, as shown in Fig. 5(b):

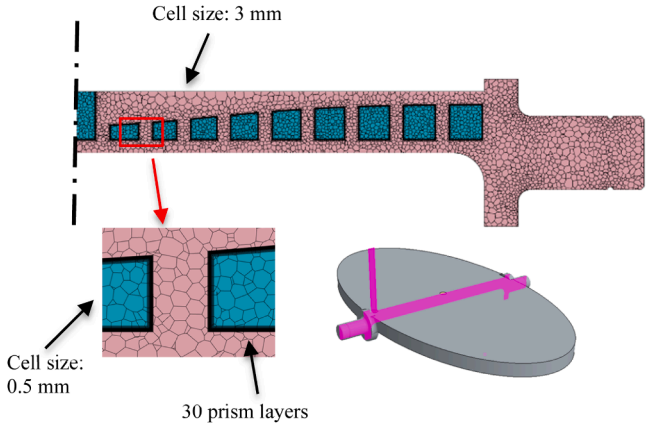

Fig. 3. Mesh configuration for CFD simulation with section view perpendicular to mirror minor axis.

- One support is fixed in all directions, both for displacement and rotation.
- The other support is left free to translate and rotate only along the x-direction.

The objective of the FSI analysis is to estimate the thermo-mechanical stresses acting on the component and the resulting deformation. As SiC is a brittle material, the Rankine criterion is considered for the evaluation of the critical stress [20]. This criterion states that failure of a component occurs when the maximum principal stress equals the material's uniaxial tension strength, or when the minimum principal stress equals the material's uniaxial compressive strength. For ceramics, and for SiC in particular, the compressive strength (~ 2000 MPa) is much higher than the tensile stress (~ 200 MPa). Moreover, compression is not associated with crack propagation. Therefore, the most representative design figure for thermo-mechanical assessment is the ratio between the ultimate tensile stress of the material and the maximum tensile stress resulting from simulation. This parameter is called the safety factor η. The condition $\eta \geq 2$ is considered for design assessment.

We can define the tensile and compressive fields as:

$$\sigma_M(x,y,z) = \max\{\sigma_1(x,y,z),\ \sigma_2(x,y,z),\ \sigma_3(x,y,z)\}$$

$$\sigma_m(x,y,z) = \min\{\sigma_1(x,y,z),\ \sigma_2(x,y,z),\ \sigma_3(x,y,z)\}$$

where σ_1, σ_2 and σ_3 are the principal stress fields. Failure occurs when one of the following conditions is met:

$$\sigma_M \geq \sigma_t \quad \sigma_m \leq \sigma_c$$

where σ_t is the ultimate tensile stress and σ_c is the ultimate compressive stress. The safety factor is hence defined as:

$$\eta = \frac{\sigma_t}{\sigma_M}$$

Using Weibull theory, the failure probability F of ceramic materials can be associated to the safety factor η via the following distribution function [21]:

$$F = 1 - e^{-\eta^{-m}}$$

where m is the Weibull modulus. The higher the Weibull modulus, the more similar the defects in the material are to one another, and the narrower the probability curve of the strength distribution.

Table 1 summarizes material properties required by the simulations and provided by the manufacturer. After defining material properties in the FSI software, setting the boundary constraints, and importing the temperature and pressure fields resulted from the CFD analysis, the simulation is executed, with the deformation and stress fields as outputs. First, although the inlet and outlet are positioned asymmetrically, the resulting pressure distribution along the channel does not induce significant rotations or deformations in the mirror. This is due both to the symmetry of the constrained supports, which helps mitigate the minor pressure contribution, and because the hydraulic load is not high enough to cause notable deformations. Secondly, Fig. 6 shows the tensile (a) and compressive (b) stress fields at steady-state, evaluated by considering the maximum and minimum among the principal stresses. The fracture limit of 220 MPa is not exceeded, with a maximum tensile stress of 128.9 MPa and a less critical compressive stress of 90.6 MPa. Moreover, it should be noticed that the maximum stress occurs at the supports due to stress concentration near the supports. Since the geometry of the constraints can be easily modified and adapted to avoid stress concentration, it is relevant to check the critical stress values in the central region of the mirror. In this case, we get a maximum tensile stress of 67.4 MPa and a maximum compressive stress of −57.8 MPa, respectively, which are well below the flexural strength. When specifically comparing the tensile stress with the flexural strength, the ratio shows a safety factor of

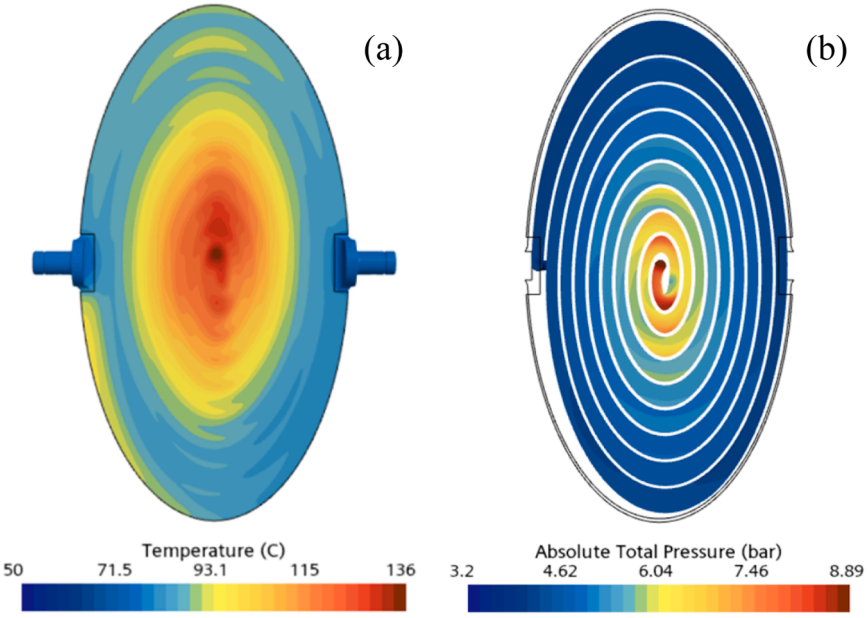

Fig. 4. Mirror temperature (a) and fluid pressure (b) profile.

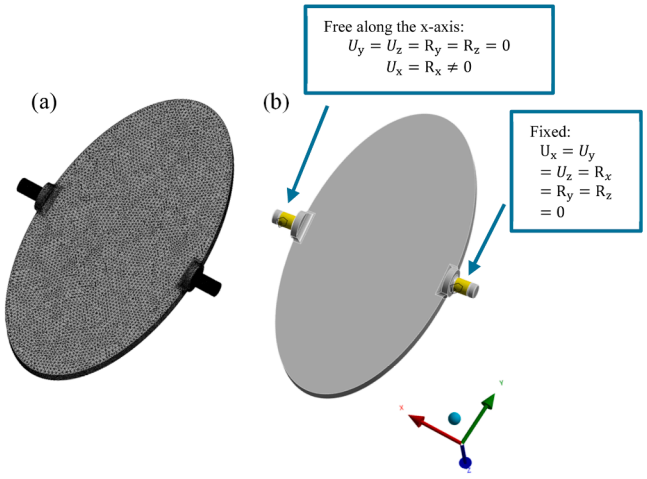

Fig. 5. Tetrahedral mesh (a) for the Finite Element Analysis (FEA). Constraints on the supports set as boundary condition (b).

Table 1
Thermo-mechanical properties of Silicon Carbide.

ρ [kg /m^3]	2950
c_p[J /(kg·K)]	700
k[W /(m·K)]	100
α[K^{-1}]	4.10^{-6}
E[GPa]	340
ν[−]	0.18
σ_t [MPa]	220
m [−]	10

3.26, well above the threshold value of 2 established as the acceptability criterion.

Fig. 7 represents the trend of the failure probability as a function of the safety factor for three values of the Weibull modulus. The safety factor calculated considering the stress experienced by the bulk mirror without supports corresponds to a failure probability of $\sim 10^{-5}$.

Fig. 8 shows the total deformation in three dimensions under steady-state condition. The maximum value of approximately 89 μm is sufficiently small to not cause issues related to changes in beam focusing. Finally, Fig. 9 displays the deformation along the z-axis, perpendicular to the mirror surface. The maximum deformation in z-direction is 30.25 μm along the minor radius and 79.60 μm along the major radius.

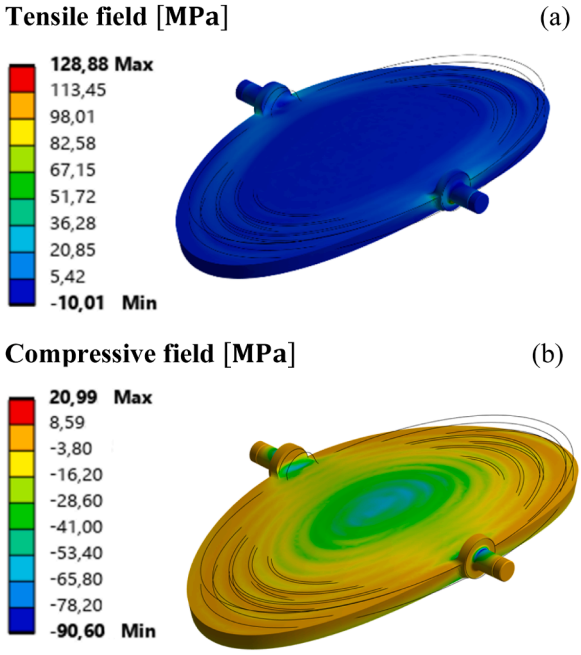

Fig. 6. Tensile (a) and compressive (b) stress fields of the M2 mirror.

The results confirm the effectiveness of the heat exchange and the capacity of the ceramic material to resist thermo-mechanical loads. Finally, tungsten, with a surface roughness of approximately 0.25 μm, exhibits thermo-mechanical properties comparable to those of the ceramic bulk material, particularly in terms of its coefficient of thermal expansion (CTE), which is critical for minimizing interfacial stresses. Consequently, it was selected as a potential coating candidate. However, deposition and adhesion experiments are still ongoing.

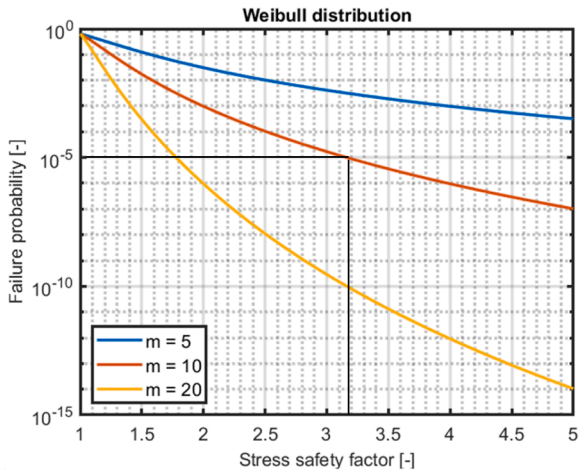

Fig. 7. Failure probability as a function of safety factor.

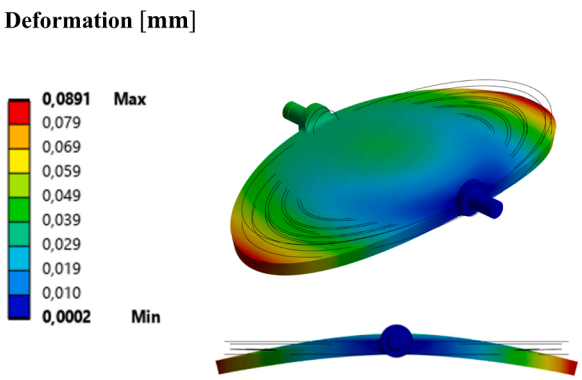

Fig. 8. Total deformation of the M2 mirror.

4. Transient thermo-mechanical analysis of M2

A transient analysis was performed on the M2 mirror to assess that the steady state condition is the most demanding from a thermo-mechanical standpoint. To speed up computation, the CFD simulation was halted at different time instants, and the stress field was computed for only those specific conditions. Despite DTT experiments will last up to 100 s, a simulation time of 3 s is sufficient to capture the transient thermal behavior of the mirror. The analysis was conducted considering three time intervals:

- Between 0 s and 0.25 s, water begins to circulate in the cooling system with a flow rate represented by a ramp that increases from 0 to 10 l/min. This approach helps to avoid issues related to computational errors that result in extremely high and erroneous mechanical stress values. Subsequently, the water is allowed to circulate until it reaches its steady-state condition.
- Between 0.25 s and 1.5 s, thermal loads are applied to analyze the heating phase of the mirror, evaluating the associated mechanical stress at various points. During this interval, the mirror reaches thermal steady-state.
- From 1.5 s to 3 s, the thermal load is interrupted, but water continues to circulate in the channel to cool the mirror. During this interval, specific points are identified where a structural analysis is performed to compute the associated mechanical stresses.

The result of the transient analysis is depicted in Fig. 10, where (a) shows the thermal peak history, while (b) displays the maximum and minimum principal stresses, representing the tensile and compressive

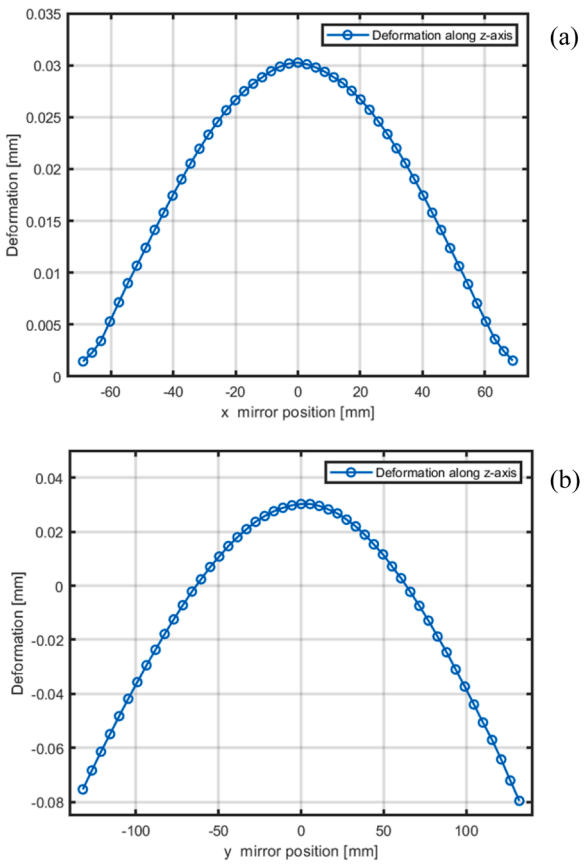

Fig. 9. Deformation along z-axis on the minor radius (x-axis, shown in a) and the major radius (y-axis, shown in b).

values, respectively. Most importantly, the highest stress values correspond to the steady-state condition in which the mirror reaches its maximum temperature; therefore, the steady-state results can be regarded as the worst-case scenario for the entire experiment.

5. Thermo-mechanical performances of different mirror materials

After analyzing the ceramic M2 mirror, a comparison was made among various materials, including CuCrZr, Aluminum T6, AISI 316 L, Inconel 718 and SiC. Since the resistance criteria differ for brittle and ductile materials, to represent the strength values on the same graph the safety factor was calculated as the ratio between the allowable stress and the critical stress on the component, as indicated by the failure criterion. For the brittle material, the maximum tensile stress is considered, while for ductile materials the equivalent Von Mises stress is taken into account. The analysis was conducted by first performing steady-state CFD simulations to obtain the worst-case scenario where the temperature reaches its peak. The results are then taken as boundary conditions in a FSI simulation to determine the stresses acting on the component and the associated safety factor. When the safety factor is greater than 1, the component is expected to resist thermo-mechanical loads; conversely, when it is <1, component failure is expected.

Fig. 11 shows a plot of the safety factor as a function of thermal conductivity, which is used as an index for the material type. It can be observed that as thermal conductivity increases, the safety factor also increases, although not necessarily in a proportional manner. The safety factor, in fact, depends not only on the thermal properties but also on the mechanical properties of the material. Clearly, the optimal situation is observed for materials with higher thermal conductivity, which correspond to a lower peak temperature; conversely, materials with low

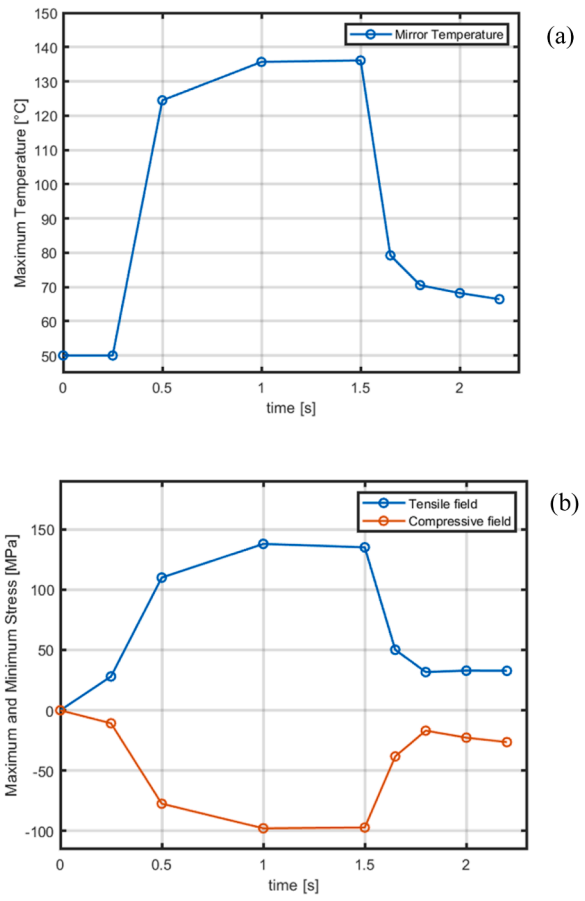

Fig. 10. Thermal (a) profile and tensile and compressive (b) profile over time.

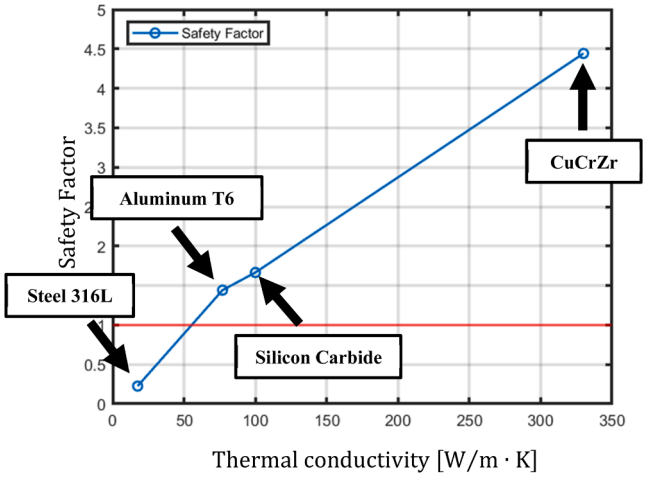

Fig. 11. Safety factor plotter for various materials to compare their mechanical strength.

thermal conductivity are characterized by a safety factor close to or lower than 1. It should be noticed that these simulations include mirror supports, where the mechanical stress is enhanced. Higher safety factors could be obtained by considering only the stress in the central region of the mirror.

6. Crack propagation analysis

An analytical assessment of the possibility of unstable crack propagation was conducted. The figure of merit for this kind of analysis is the fracture toughness of the material K_{IC}. From this value, it is indeed possible to calculate the admissible stress to prevent crack propagation. Based on experimental formulas found in the literature, the limit stress value σ_{max} that triggers crack propagation can be calculated for different crack sizes c [22]. The formula used is as follows:

$$K_I = \sigma_{max} \cdot \beta \cdot \left(\sqrt{c \cdot \pi}\right)$$

The fracture toughness of SiC is assumed to be 2 $[MPa\sqrt{m}]$, K_I is the stress intensity factor in mode I, while β is a correction factor that takes into account the geometry of the crack, which in this case is assumed to be equal to 1.12, corresponding to a crack on the surface [22]. The graph in Fig. 12 shows the trend of the K_I as a function of crack size. Fracture occurs when K_I reaches a critical value: $K_I = K_{IC}$.

In this case, the maximum tolerable crack size for the material under the peak stress of 67.5 MPa is $\approx$ 0.2 mm. Furthermore, the graph was created by considering stress values corresponding to various points on the mirror, subjected to different levels of stress. Indeed, for a constant K_I value defined by the material, the crack size can increase as the stress decreases. To be conservative, the reference value is the most highly stressed area of the mirror with a crack size of approximately 2 mm. Therefore, unstable crack propagation is not expected as defects of large size could be detected by non-destructive methods during commissioning of the mirror.

7. Thermo-mechanical analysis of the test mirror

Through CFD and FSI simulations, the suitability of a SiC dielectric substrate for the M2 mirror was assessed. The next step is to procure a 1:1 prototype mirror to be tested in realistic conditions, in order to validate the design and assess mirror resistance to thermal loads, fluid dynamic conditions, and mechanical stresses. The experiments are planned at the FALCON facility of the Swiss Plasma Center at EPFL [23], under realistic conditions using high-power microwave sources with the same features as the DTT ECH system ones and a Connection Line section specifically designed and procured for these tests [24]. For compatibility with the rest of the microwave transmission line envisioned for the experiments, the prototype has slightly different geometry with respect to M2. In fact, as shown in Fig. 13(b), the reflective front surface of the prototype is not flat, but concave; the major and minor radii of the elliptical perimeter are 89 mm and 63 mm, respectively, while the inlet and outlet diameters of the cooling channel are 7 mm wide. Four rear bolted joints will be used to secure the mirror to the supporting structure. The cooling system developed for the M2 mirror has been adapted and tailored to fit the different geometry of the test mirror, preserving

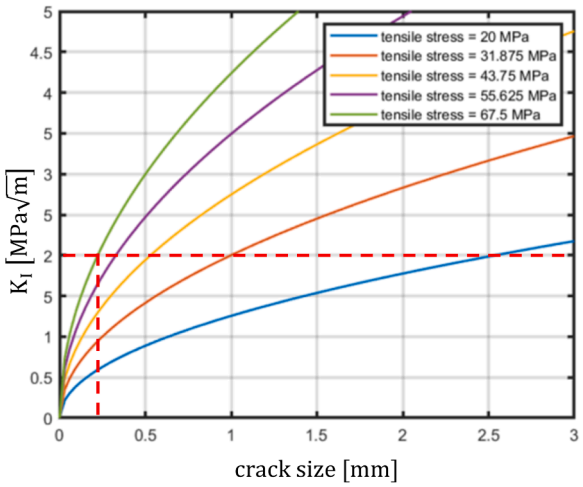

Fig. 12. Admissible stress as a function of crack size.

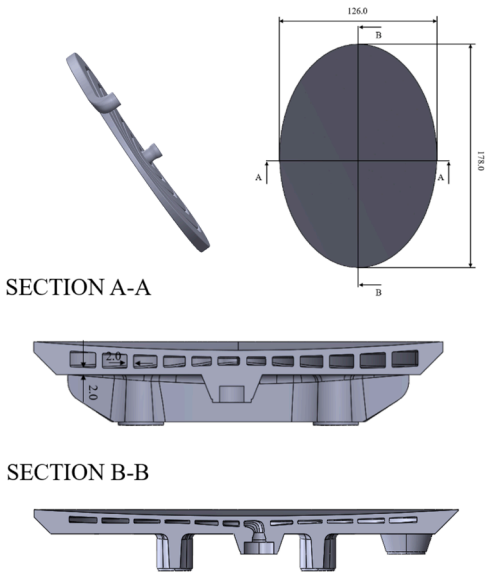

Fig. 13. (a) Internal variable-depth complementary spiral (VDCS) cooling channel adapted to the test mirror. (b) Test Mirror size and section view.

the Gaussian-sinusoidal pattern of the path to accurately reproduce the system's fluid dynamics. Fig. 13(a) shows the cooling channel for the test mirror.

Steady-state CFD and FSI simulations were conducted on the prototype mirror following the same steps outlined in Sec. III. However, the boundary conditions are modified according to the envisioned specifications of the testing facility:

- The inlet flow rate is set at 5 l/min
- The inlet temperature is set at 15 °C
- The outlet pressure is set at 4 bar.
- The thermal load of microwaves has a Gaussian profile with $w_x = 31.32$ mm, $w_y = 44.29$ mm and a central peak of 2.86 MW $/m^2$

The mesh of the model is shown in Fig. 14(a). In Fig. 14(b and c), the thermal and fluid dynamic results are shown. Despite the higher heat flux compared to the M2 mirror, the thermal and fluid dynamic results fall within the operability range: the maximum temperature on the mirror is approximately 163.03 °C, while water reaches a maximum temperature of 117.94 °C, well below saturation conditions and thus far from the onset of boiling. Finally, the pressure drop along the channel is 1.03 bar. Based on the thermal analysis, FSI structural simulations are then performed to assess the mechanical resistance of the component, considering the properties of SiC summarized in Tab. 1. The employed tetrahedral mesh is shown in Fig. 15(a).

The mechanical boundary conditions represent the rear supports used to fix the mirror. As shown in Fig. 15 (b, c, d), three alternative cases were considered in this analysis to study the effect of the constraints and to evaluate the stresses acting on the mirror under different operating conditions:

- Four supports are fixed in all directions (b).
- One support is fixed in all directions and three supports are constrained along the z-axis perpendicular to the mirror (c).
- One support is fixed in all directions, and three supports are allowed to move and rotate freely in all directions (d).

For each examined case, the Rankine criterion for brittle materials is used. The resulting maximum and minimum stresses are displayed in Fig. 16, representing the tensile and compressive values, respectively, along with the associated deformation.

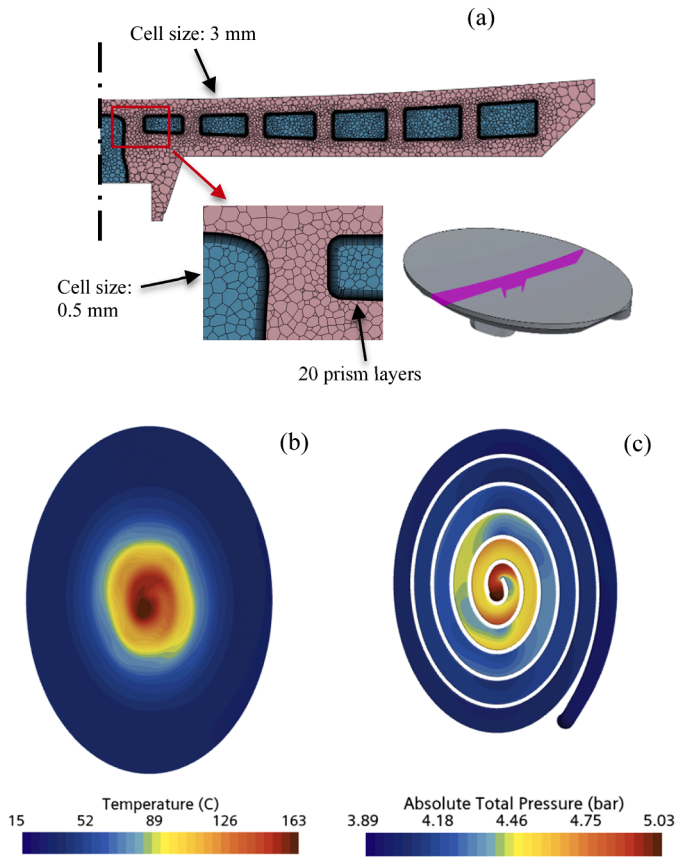

Fig. 14. Mesh configuration (a) for CFD simulation with section view perpendicular to mirror minor axis. Mirror (b) temperature and fluid (c) pressure profile.

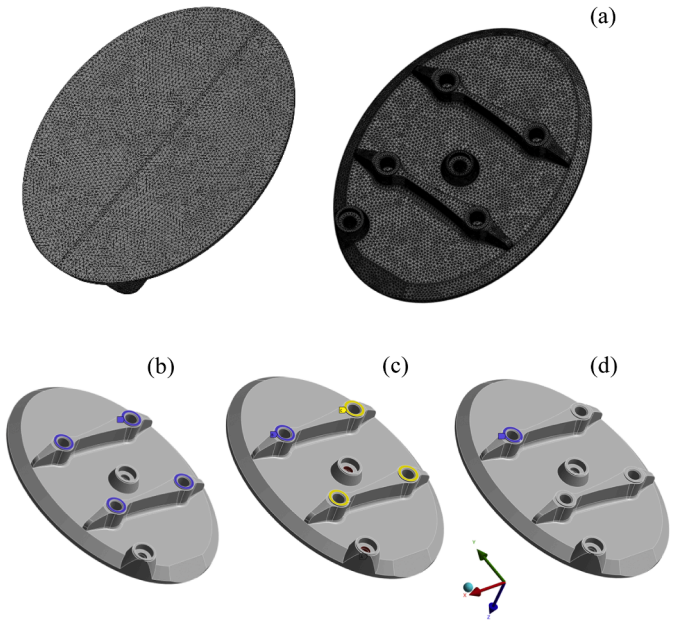

Fig. 15. Tetrahedral mesh (a) for the Finite Element Analysis (FEA). Constraints on the supports set as boundary condition for the three different cases (b, c, d).

In this case, the maximum stress is compressive, with an absolute value of 134.77 MPa for the scenario where the mirror has one fixed support and the other three are constrained along the z-axis, perpen-

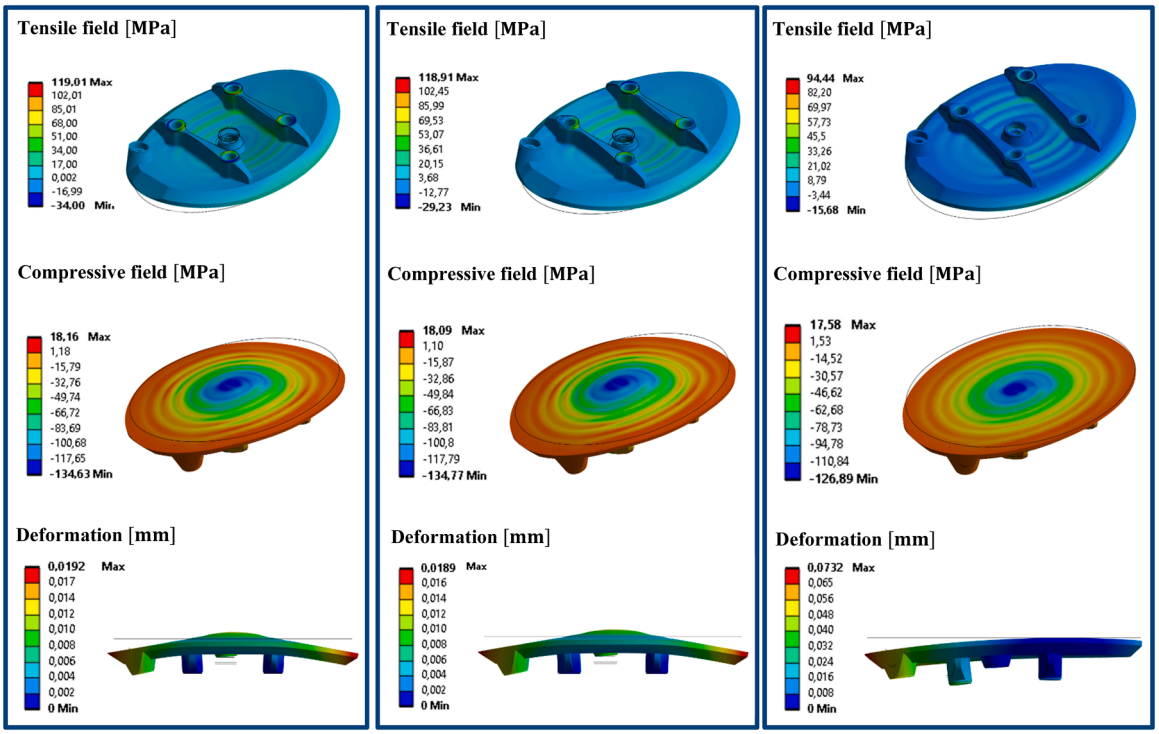

Fig. 16. Tension and Compressive stress fields and total deformation, respectively, for the three cases of boundary conditions introduced earlier.

dicular to the mirror. This corresponds to a maximum deformation of 18.93 μm By progressively relaxing the degrees of freedom of the constraints, the mechanical stresses are reduced, resulting in higher deformations. Indeed, in the case where only one support is fixed while the others are completely free, the highest mechanical stress experienced by the mirror is again compressive, with a value of −126.89 MPa, corresponding to a maximum deformation of 73.21 μm Finally, as with the M2 mirror, a possible coating material was investigated for the prototype. Given the thermo-mechanical properties of tungsten, which are similar to those of the mirror's bulk material, it was evaluated as a potential candidate for the prototype as well.

8. Conclusions

This paper illustrates the thermo-mechanical analysis of a dielectric substrate of the M2 mirror made of Silicon Carbide. The internal cooling channel of the mirror, featuring an optimized Variable-Depth Complementary Spiral geometry, was studied along with the proposed substrate material to suppress the magnetic torques acting on the mirror.

Considering that ceramics are brittle materials, the tensile and compressive principal stress fields acting on the mirror were compared with the strength of the material according to the Rankine criterion, after applying proper boundary conditions.

A transient thermo-mechanical analysis capturing the essential cooling transients as well as the steady-state condition, was setup. From this analysis, we observe that the worst-case scenario is the steady-state condition in which the temperature of the mirror reaches its peak value along the entire experiment. Therefore, subsequent analyses only considered the steady-state scenario, thereby lowering the computational cost.

Steady-state CFD analyses demonstrated that a SiC substrate can keep the temperature of the mirror and water pressure drops within acceptable levels. Mechanical resistance was tested through FSI analyses by coupling the thermo-fluid dynamic solver with the mechanical solver in ANSYS. The results demonstrate the theoretical integrity of the new design, both from a thermal and a mechanical perspective.

Subsequently, different materials were compared in terms of thermo-mechanical resistance to the foreseen thermal loads. The Von Mises failure criterion was employed to compute the safety factor associated with ductile materials. The comparison shows that silicon carbide, despite its brittleness, can withstands thermo-mechanical stresses better than stainless steel and even Aluminum, further supporting the suitability of the proposed solution.

In addition, an analytical assessment of unstable crack propagation was conducted. The fracture toughness of SiC was considered and the graph of the admissible stress as a function of superficial crack size was obtained. Given the relatively low stresses acting on the mirror, cracks with size lower than 0.2 mm would not undergo unstable propagation, while larger cracks would be easily detectable by non-destructive methods during commissioning.

Lastly, the geometry of a prototype mirror for experimental testing was developed. CFD and FSI analyses on the prototype geometry revealed acceptable thermo-mechanical performance, which serves both as an assessment of the feasibility of the experiments, and as a dataset for model validation.

CRediT authorship contribution statement

Alfredo Pagliaro: Conceptualization. **Francesco Braghin:** Supervision. **Alessandro Bruschi:** Supervision. **Daniele Busi:** Supervision. **Eliana De Marchi:** Supervision. **Francesco Fanale:** Supervision. **Gustavo Granucci:** Supervision. **Afra Romano:** Supervision. **Fabio Zanon:** Supervision.

Declaration of competing interest

The authors declare the following financial interests/personal relationships which may be considered as potential competing interests:

Daniele Busi reports financial support was provided by Eni SpA. Francesco Braghin reports financial support was provided by Eni SpA. Alfredo Pagliaro has patent pending to CNR, ENI, POLITECNICO of MILANO. If there are other authors, they declare that they have no

known competing financial interests or personal relationships that could have appeared to influence the work reported in this paper.

Acknowledgements

The work was carried out as part of the DTT activities, in the context of Eni-CNR JRA. The authors wish to thank all colleagues involved in the project for their precious contributions to its completion.

The paper deals with the filed patent application for a “device and use of the device for reflecting microwave radiation during electron-cyclotron resonance heating”.

Data availability

The data that has been used is confidential.

References

[1] F. Romanelli, et al., Divertor Tokamak Test facility project: status of design and implementation, Nucl. Fusion 64 (Sept 2024), https://doi.org/10.1088/1741-4326/ad5740.
[2] S. Garavaglia, et al., Progress of DTT ECRH system design, Fusion Eng. Des. 168 (Jul. 2021) 112678, https://doi.org/10.1016/J.FUSENGDES. 2021.112678. Art. no.
[3] F. Fanale, et al., Status of DTT ECH Transmission lines and Antennae, IEEE Trans. Plasma Sci. (Apr. 2024), https://doi.org/10.1109/TPS.2024.3382745.
[4] A. Moro, et al., Progress and challenges of the ECH transmission line design for DTT, Fusion Eng. Des. 202 (May. 2024), https://doi.org/10.1016/J.FUSENGDES.2024.114391.
[5] D. Busi, et al., In-vessel piezoelectric actuation system for DTT ECRH launchers: conceptual design, Fusion Eng. Des. 180 (Jul. 2022) 113196, https://doi.org/10.1016/J.FUSENGDES.2022.113196. Art. no.
[6] E. Gajetti, et al., A new efficient mirror cooling for the transmission line of fusion reactor ECH systems based on triply periodic minimal surfaces, IEEE Trans. Plasma Sci. (Apr. 2024), https://doi.org/10.1109/TPS.2024.3383275.
[7] X. Wang, et al., Research activities and progress on the long pulse ECRH launcher for EAST, in: Proc. EPJ Web Conf, 2019 02012, https://doi.org/10.1051/epjconf/201920302012.
[8] M. Joung, et al., Design of ECH launcher for KSTAR advanced Tokamak operation, Fusion Eng. Des. 151 (Feb. 2020) 111395, https://doi.org/10.1016/J.FUSENGDES.2019.111395. Art. no.
[9] V. Erckmann, et al., Electron cyclotron heating for W7-X: physics and technology, Fusion Sci. Technol. 52 (Aug. 2007), https://doi.org/10.13182/FST07-A1508.
[10] H. Hailer, et al., Mirror development for the 140 GHz ECRH system of the stellarator W7-X, Fusion Eng. Des. 66-68 (Sep. 2003) 639–644, https://doi.org/10.1016/S0920-3796(03)00264-3, vols.
[11] A.Mas Sanchez, et al., Fluid-dynamic and thermo-mechanical analyses of the ITER electron cyclotron Miter bend mirror for the off-centered beam scenario, Fusion Eng. Des. 192 (Jul. 2023) 113643, https://doi.org/10.1016/J.FUSENGDES.2023.113643. Art. no.
[12] F. Sanchez, et al., Design and manufacturing of the ITER ECRH upper launcher mirrors, Fusion Eng. Des. 84 (Jun. 2009) 1702–1707, https://doi.org/10.1016/J.FUSENGDES.2009.01.013.
[13] P.Santos Silva, et al., Design concept and thermal-structural analysis of a high power reflective mm-wave optical mirror (M2) for the ITER ECH-UL, Fusion Eng. Des. 146 (Sep. 2019) 618–621, https://doi.org/10.1016/J.FUSENGDES.2019.01.037.
[14] D. Busi, et al., Study of magnetic effects on DTT ECRH front-steering mirror, Fusion Eng. Des. 191 (Jun. 2023) 113550, https://doi.org/10.1016/J.FUSENGDES.2023.113550. Art. no.
[15] A. Pagliaro, et al., Variable-depth complementary spiral cooling channel design for the steerable ECRH mirrors of DTT, submitted to *Fusion Eng. Des.* 219 (Oct. 2025) 115276, https://doi.org/10.1016/j.fusengdes.2025.115276. Art. no.
[16] Siemens CD-adapco. *STAR-CCM+User Guide*. 2020.
[17] B. Bird, “Transport phenomena”, 2001.
[18] P. Goldsmith, Quasioptical Systems, IEEE Press, 1998.
[19] A. Salvitti, et al., Preliminary design and thermal analyses of the steerable mirror cooling channel of the DTT ECRH, Fusion Eng. Des. 161 (Dec. 2020) 111880, https://doi.org/10.1016/J.FUSENGDES.2020.111880. Art. no.
[20] B.K. Yildiz, Assessment of mechanical performance of Al_2O_3 ceramic honeycomb sandwich structures produced with SLA 3D-printing regarding unpolymerized slurry removal strategy, J. Aust. Ceram. Soc. 60 (2024) 1199–1208, https://doi.org/10.1007/s41779-024-01021-x. Apr.
[21] S.L. Fok, et al., A numerical study on the application of the Weibull theory to brittle materials, Eng. Fract. Mech. 68 (Jul. 2001) 1171–1179, https://doi.org/10.1016/S0013-7944(01)00022-4.
[22] C.H. Wang, Introduction to fracture mechanics, DSTO Aeronaut. Marit. Res. Lab. (Jul. 1996). DSTO-GD-0103.
[23] École Polytechnique Fédérale de Lausanne, Swiss Plasma Center website (https://www.epfl.ch/research/domains/swiss-plasma-center/research/tcv/research_tcv_heating/tcv-ecrh-eccd-system/).
[24] S. Garavaglia, et al., "First RF operations of the gyrotron for DTT ECRH system", submitted to *Fusion Eng. Des.*